Journal of Advanced Ceramics
2014, 3(1): 17–30
DOI: 10.1007/s40145-014-0089-x

ISSN 2226-4108
CN 10-1154/TQ

Research Article

Effect of sintering temperature on microstructure and electrical properties of $Sr_{1-x}(Na_{0.5}Bi_{0.5})_xBi_2Nb_2O_9$ solid solutions

Hana NACEUR*, Adel MEGRICHE, Mohamed EL MAAOUI

Laboratory of Applied Mineral Chemistry, *Department of Chemistry*, *Faculty of Sciences*, *University Tunis ElManar*, *Campus 2092*, *Tunis*, *Tunisia*

Received: September 13, 2013; Revised: November 14, 2013; Accepted: November 18, 2013

Abstract: In this study, we investigated the effect of sintering temperature on densification, grain size, conductivity and dielectric properties of $Sr_{1-x}(Na_{0.5}Bi_{0.5})_xBi_2Nb_2O_9$ ceramics, prepared by hydrothermal method. Pellets were sintered at different temperatures. Density increased with sintering temperature, reaching up to 96% at 800 ℃. A grain growth was observed with increasing sintering temperature. Impedance spectroscopy analyses of the sintered samples at various temperatures were performed. Increase in dielectric constant and in Curie temperature with sintering was discussed. Electrical conductivity and activation energy were calculated and attributed to the microstructural factors.

Keywords: ceramics; sintering; light scattering; dielectric properties

1 Introduction

Dielectric and ferroelectric ceramic materials are mature and ubiquitous materials for advanced technology. These ceramics are active elements in a range of dielectric devices and performing functions such as sensing and actuation. Recently, ferroelectric material of strontium bismuth niobate $SrBi_2Nb_2O_9$ (SBN) and its solid solutions have attracted much attention for potential applications in the field of nonvolatile random access memory (NVRAM) due to their excellent fatigue endurance and low switching voltage. The performance of these materials is closely related to their microstructures and, for this reason, to the ways they have been processed. Preparation condition, especially sintering temperature is an important factor in the fabrication process of ceramic bodies, which can significantly affect the mechanical and electrical properties of materials [1,2]. For improvement of these properties, parameters affected by sintering such as density, porosity, grain size and their distribution must be controlled [3,4]. In fact, sintering, as one of the most important processes for the production of ceramic materials, usually goes through a sequence of essential phenomena such as neck formation, pore, shrinkage, and grain growth. It results in a solid compact with a suitable microstructure. During the sintering of a powder compact, both densification and grain growth occur simultaneously [5]. It is necessary to control the total densification process of the material as well as the pore presence and to avoid grain growth, which require a full understanding of the material constitutive laws

* Corresponding author.
E-mail: Naceur.hana@live.fr

governing the sintering process.

There are numerous reports on the synthesis of bismuth niobate and its solid solutions by processes such as solid-state reaction [6–8], aqueous solution method [9,10], organic precursor decomposition [11,12], co-precipitation [13–15], sol–gel [16,17], and combustion synthesis [18] which often results in high agglomeration of powders. For these several chemical synthesis routes, a high sintering temperature is usually necessary for the densification of ceramics [19]. It often causes a variation in the stoichiometry ceramics and in the production of a liquid phase, caused by volatilization of Na_2O, Bi_2O_3, etc.

Density can be improved through the use of sintering aids [20]. In fact, further studies on sintering behavior reveal that adding excess amounts of Bi_2O_3 in the processing of many compounds could facilitate the densification process [21]. Increasing the amount of Bi_2O_3 addition and sintering temperature enhancs the development of the preferred orientation and coarsening of grains [21]. In a recent work for $BaTiO_3$ compound, the addition of small amounts of Li_2O to various ceramics has been reported to lower the sintering temperature by various mechanisms [22]. In another recent work, an addition of H_3BO_3 effectively lowers the sintering temperature of $Li_2ZnTi_3O_8$ ceramics from 1075 ℃ to 880 ℃ [23]. Many reports reviewed the hot pressing and the spark plasma (sintering) [24–26] for densification of ceramics; however, these methods are unsuitable for stress and impurity-free ceramics. One of the main challenges is the difficulty of producing dense ceramics using ordinary firing methods. A solid state double sintering method is employed in many works involving two-step firing [27–29]. The first step, at relatively low temperature, is to promote the chemical reactions among the constituent compounds so as to form a single phase layered perovskite. The second step, firing at high temperature, is to achieve high densification. In order to use moderate sintering temperatures and attain low porosity, recently, a first study on microwave sintered $SrBi_2Ta_2O_9$ ceramic was reported [30].

Hydrothermal synthesis of ceramic powders has gained considerable popularity. This process progresses in a closed system at a high autogenous pressure and leads to high-quality powders, with well-controlled morphology and narrow particle size distribution [31]. The hydrothermal synthesis is sometimes called “soft chemical processing solution” because of the mild reacting conditions under which the products are achieved, leading to controlled particle size and morphology. These characteristics decrease the sintering temperatures and, consequently, low-price products can be obtained [32]. It is thus regarded as a promising way to prepare bismuth niobate powders with a low sintering temperature, which is beneficial to obtain easily controlled-size grains, adjust the compound stoichiometry and reduce the volatilization of alkaline elements [33]. A novel hydrothermal apparatus with ball milling system is developed by Hotta *et al*. to produce nanosized $BaTiO_3$ powders with low-temperature sintering capability [34].

Therefore, there is a considerable interest in the search of new dielectric materials with low sintering temperature [35,36]. Our recent work stated a particular point concerning the sintering temperature for $Sr_{1-x}(Na_{0.5}Bi_{0.5})_xBi_2Nb_2O_9$ pellets at 800 ℃ [37]. Powders synthesized by hydrothermal method are lowly sinterable. This temperature appears to be sufficient to perform a good densification despite the fact that samples are usually sintered at temperature higher than 1000 ℃ [35,38].

The main objective of this work is to develop the effect of sintering temperature on densification, shrinkage and grain size. These parameters have pronounced influence on the device properties of materials. Density of $Sr_{1-x}(Na_{0.5}Bi_{0.5})_xBi_2Nb_2O_9$ pellets at different sintering temperatures is determined. The morphology of different sintered powders is discussed. Their electrical conductivity and activation energy are characterized and compared. The variation of Curie temperature and dielectric constant in function of sintering temperatures for all compositions is evaluated.

2 Experiment

The $Sr_{1-x}(Na_{0.5}Bi_{0.5})_xBi_2Nb_2O_9$ powders with different x values ($x = 0.0$, 0.2, 0.5, 0.8 and 1.0) were synthesized by the hydrothermal process. The preparation was detailed in our recent report [37].

Pellets were prepared by pressing the powder samples at 10 tons. The thickness and the diameter were about 1.6 mm and 13 mm, respectively. These disks were sintered at different temperatures in a programmable furnace (Vulcan, Model 3-550) and the heating rate was 5 ℃/min.

The pellet densities were measured before sintering (called green density ρ_g) and after sintering (called sintered density ρ_s), in water using the Archimedes principle as follows:

$$\rho_{g/s} = \frac{M_a}{(M_b - M_W) \times \rho_W} \quad (1)$$

where M_a is the mass of the sample in air; M_b is the mass of the sample in air after submerged from water; M_W is the mass of the sample in water; ρ_W is the density of water; and $\rho_{g/s}$ is the green or the sintered density.

The theoretical density (ρ_t) was calculated from the diffraction patterns applying the formula:

$$\rho_t = \frac{\text{Cell mass}}{\text{Cell volume}} = \frac{n \times M_S}{N \times a \times b \times c} (\text{g/cm}^3) \quad (2)$$

where n is the number of atoms per unit cell; M_S is the molecular weight of the compound; N is the Avogadro number; and a, b and c are the lattice parameters of orthorhombic sample refined by the least square method from the powder data.

The density percentage ($\rho_s(\%)$) after sintering was carried out using the following formula:

$$\rho_s(\%) = \left(\frac{\rho_s}{\rho_t}\right) \times 100 \quad (3)$$

A densification factor (DF) for all sintered pellets can be related with sintered density, green density and theoretical density, with the following expression:

$$\text{DF} = \frac{\rho_s - \rho_g}{\rho_t - \rho_g} \quad (4)$$

It is worthwhile giving thought on the changes that occur in a ceramic body during sintering. The shrinkage measurements were determined for all samples by the diameter and thickness reduction. The percentages of the diameter and thickness reduction were calculated using these two equations:

$$\text{Diameter shrinkage} = \left(\frac{d_0 - d_f}{d_0}\right) \times 100\% \quad (5)$$

$$\text{Thickness shrinkage} = \left(\frac{h_0 - h_f}{h_0}\right) \times 100\% \quad (6)$$

where d_0 is the diameter before sintering; d_f is the diameter after sintering; h_0 is the height before sintering; and h_f is the height after sintering.

In order to estimate average grain size, a suspension of the obtained product was measured by a dynamic light scattering (DLS) technique, calculated by the Stocks–Einstein relation [39]:

$$G_i = \frac{k_B \times T}{3\pi \times \eta_s \times D} \quad (7)$$

where D is the diffusion coefficient; k_B is the Boltzmann constant; T is the absolute temperature; η_s is the viscosity coefficient of solvent; and G_i is the mean grain size.

Measurements were carried out at 90° over a temperature range of 10–50 ℃ using a variable angle light scattering instrument equipped with an Excel 3000 argon ion laser (1200 mW at 514.5 nm) as the source and a Brookhaven Digital BI 2030AT correlator.

The dielectric constant and the Curie temperature were deducted for the sintered ceramic pellets, using an HP 4192A impedance gain phase analyzer. The electrical conductivities of the samples were measured. The activation energies were calculated using traditional Arrhenius equation:

$$\sigma = (\sigma_0 / T) \exp[-E_a / (k_B \times T)] \quad (8)$$

where E_a is the activation energy for conduction; T is the absolute temperature; k_B is the Boltzmann constant; and σ_0 is the pre-exponential factor.

3 Results and discussion

3.1 Densification and microstructure

3.1.1 Densification

In order to improve the properties of ceramics for either structural or functional applications, reducing the grain size and limiting the formation of defects are important. During the sintering period, a considerable microstructural development takes place. Garcia *et al*. [40] reported a detailed study for the relation between the microstructure and densification of ceramics and the control of the process responsible for the rates of densification and grain growth, by controlling the time/temperature conditions employed during sintering of the compact powders.

Firstly, theoretical densities were calculated for all solid solutions by means of their lattice parameters (detected in our previous study) [37]. It is noted that these densities increase from 7.251 g/cm^3 for SBN to 7.375 g/cm^3, 7.502 g/cm^3, 7.608 g/cm^3 and 7.678 g/cm^3 for x = 0.2, 0.5, 0.8 and 1.0, respectively.

All samples with different dopings were pressed into pellets and sintered for 2 h at different temperatures from 700 ℃ to 900 ℃. Green and sintered density

values were performed by the Archimedes method. Evolution of sintered density percentage for different compositions as function of sintering temperature is plotted in Fig. 1. It could be observed that the sintering curves of all solid solutions are similar; their densities increase initially with increasing sintering temperature until 800 ℃ reaching their maximum values and remain constant up to 820 ℃, then decrease slightly for all solid solutions. Thus, the sintering of $Sr_{1-x}(Na_{0.5}Bi_{0.5})_xBi_2Nb_2O_9$ ceramics is completed at the low temperature of 800 ℃. It is well known that the process of sintering has three stages [41–43]: the initial, the intermediate, and the final one. In the initial stage, the green body has a low density and is generally lacking in physical integrity. There is a small degree of adhesion between adjacent particles. Then, the necks begin to form at the contact points. The final stage of sintering begins when most of the pores are closed.

However, beyond 820 ℃, a decrease on the density occurs on the pellets for all compositions. This phenomenon might be associated with the loss of bismuth oxide during the sintering stage. In other words, for SBN and its solid solutions, the increase of the sintering temperature is not favorable due to possible Bi loss; the melting point of Bi_2O_3 is about 825 ℃ [44] which significantly changes the density of the final ceramic. Looking away, the more the sintering temperature increases, the more the density decreases. The deviation from the stoichiometry is possible because of the vapor pressure of elements like Na^+. Na_2O loss starts to appear only above 850 ℃ and at a much higher rate at higher temperatures (> 1000 ℃) [45]. For $x = 1.0$ at 840 ℃, a variation of density at different sintering durations for 2 h, 3 h, 4 h and 5 h is plotted in Fig. 2. The increase of the sintering duration induces a decrease in density, which confirms the increase in loss of bismuth. As a result, sintering above 800 ℃ corresponds to saturation density value; all compositions are fully densified by sintering at this temperature. Thus, the hydrothermal synthesis is promising to obtain a high density at low sintering temperature. Therefore, sintered samples prepared from SBN powders, produced by hydrothermal synthesis, show a higher density than that prepared from solid-state synthesis [7]. In recent data [46], it has been found that co-precipitated $La_{0.8}Ca_{0.2}Cr_{0.9}Al_{0.1}O_3$ powders achieve a relative density of 92% after sintering at 1400 ℃ for 5 h in air. This relative density is lower than that obtained by the hydrothermally derived fine $La_{0.8}Ca_{0.2}Cr_{0.9}Al_{0.1}O_3$ powders (97%). It is obvious that generally densification is affected by the used method of preparation of the starting powders. This implies that hydrothermal method offers the potential of enhanced densification and decreased sintering temperature [46,47]. Furthermore, porosity of the crude pellet resulting from hydrothermal powder is much smaller than that attained by pressing larger grains (from other synthesis methods).

From Fig. 1, it can be also observed that sintered materials show densities significantly dependent on the composition. The saturated density values at 800 ℃ for $x = 0.0$, 0.2, 0.5, 0.8 and 1.0 are 6.933 g/cm^3, 7.057 g/cm^3, 7.181 g/cm^3, 7.295 g/cm^3 and 7.371 g/cm^3, respectively, which are equivalent to 95.62%, 95.7%, 95.73%, 95.89% and 96% of the theoretical density.

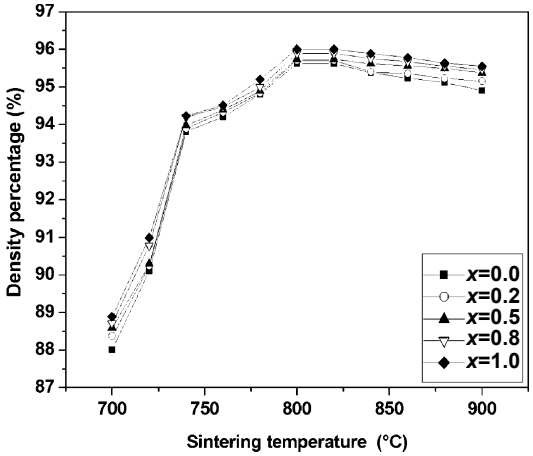

Fig. 1 Sintered density percentage as function of sintering temperature for $Sr_{1-x}(Na_{0.5}Bi_{0.5})_xBi_2Nb_2O_9$ solid solutions.

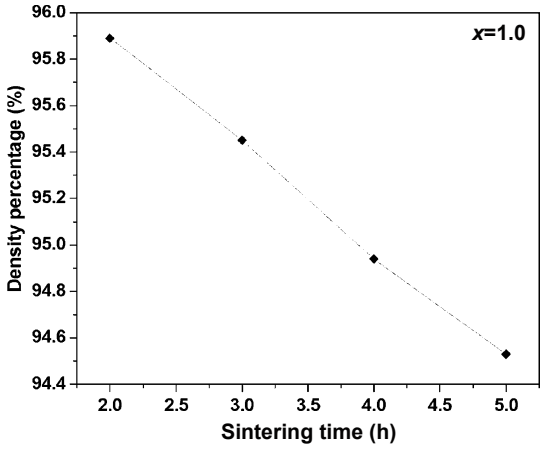

Fig. 2 Sintered density percentage as function of sintering duration at 840 ℃ for $Na_{0.5}Bi_{2.5}Nb_2O_9$ ceramic.

One can consider that the variation from 95.62% to 96% is not significant being into the error interval. In fact, three series of measurements confirm the obtained values. It appears that the addition of $Na_{0.5}Bi_{0.5}$ improves the densification process, and there is higher value of about 96% of the theoretical value for $x=1$ than the un-doped SBN. The introduction of $Na_{0.5}Bi_{0.5}$ is thus beneficial to the densification of pellets. The addition of $Na_{0.5}Bi_{0.5}$ into the system suggests that this doping can suppress the occurrence of defects [37].

Figure 3 presents the densification factor (DF) as function of sintering temperature for all solid solutions. Two comments are revealed: the first is that DF increases with $Na_{0.5}Bi_{0.5}$ increasing; the second is DF increases with increasing temperature until 800 ℃, where it remains constant then decreases for sintering temperatures higher than 820 ℃ for all solid solutions. A positive DF indicates shrinkage. The shrinkage during sintering is a result of densification mechanisms, and during cooling it is a result of thermal contraction. Yahya *et al*. [48] proved that shrinkage is the phenomenon of sintering. The shrinkage is thus only dependent on thermal dilatation. It is determined by the diameter and thickness reduction. Figure 4 shows the thickness shrinkage percentage of the pellets as function of sintering temperature. An increasing progress from 4.14% to 5.2% as the sintering temperature is increased from 700 ℃ to 800 ℃ for SBN , 4.58% to 5.48%, 4.61% to 5.55%, 4.64% to 5.58% and 4.73% to 5.64% for $x=0.2$, 0.5, 0.8 and 1.0, respectively. The diameter shrinkage percentage is plotted in Fig. 5. As shown, at the same range of temperature, it increases from 5.28% to 5.72% for SBN, 5.44% to 5.93%, 5.49% to 6.22%, 5.73% to 6.29%, 5.83% to 6.54% for $x=0.2$, 0.5, 0.8 and 1.0, respectively. That means the higher the temperature and the $Na_{0.5}Bi_{0.5}$ content are, the denser the products are; in fact, as the mass is supported to be constant, shrinkage is observed when the pellet volume decreases. This is obviously due to the pore collapse. The increased shrinkage of $Na_{0.5}Bi_{2.5}Nb_2O_9$ sample at 800 ℃ implies that both the $Na_{0.5}Bi_{0.5}$ dopant and the increase in sintering temperature promote the densification.

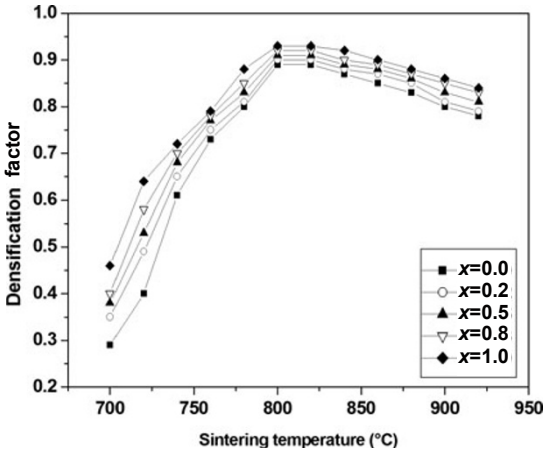

Fig. 3 Densification factor as function of sintering temperature for $Sr_{1-x}(Na_{0.5}Bi_{0.5})_xBi_2Nb_2O_9$ solid solutions.

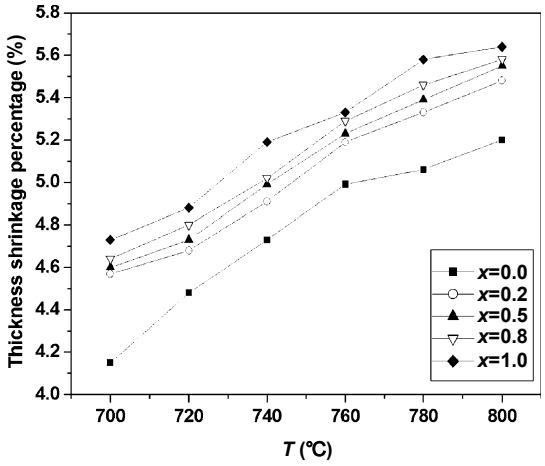

Fig. 4 Thickness shrinkage percentage as function of sintering temperature for $Sr_{1-x}(Na_{0.5}Bi_{0.5})_xBi_2Nb_2O_9$ solid solutions.

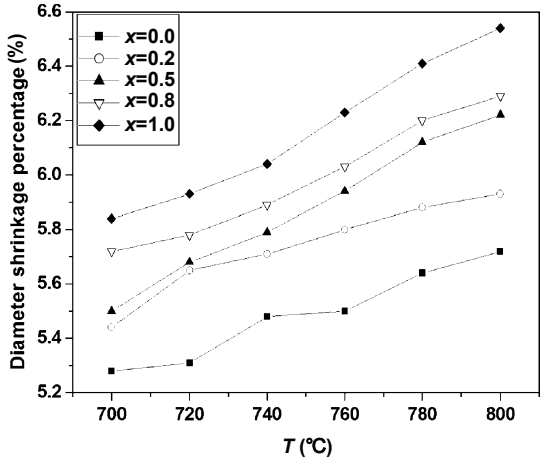

Fig. 5 Diameter shrinkage percentage as function of sintering temperature for $Sr_{1-x}(Na_{0.5}Bi_{0.5})_xBi_2Nb_2O_9$ solid solutions.

3.1.2 Grain size measurements

The grain sizes of $Sr_{1-x}(Na_{0.5}Bi_{0.5})_xBi_2Nb_2O_9$ solid solutions, determined from DLS measurements before sintering are 13 nm for SBN, 25 nm, 34 nm, 48 nm and

65 nm for $x = 0.2$, 0.5, 0.8 and 1.0, respectively .

Mean grain sizes after sintering for all compounds as function of sintering temperature are plotted in Fig. 6. Two main observations can be inferred from this graph. First, the grain size increases with increasing $Na_{0.5}Bi_{0.5}$. This anisotropic behavior of grain growth was noted in our recent work for the sintering temperature equal to 800 ℃ [37]. This grain growth behavior is general whatever the sintering temperature is. This result suggests that $Na_{0.5}Bi_{0.5}$ dopant speeds up the grain growth [37]. It is due to a flux effect resulting from the introduced Na^+ and Bi^{3+}. These cations are well known for their flux behavior. It is also possible to involve the effect of solute drag on the grain boundaries [49]. Thus, migration of cation impurities to the grain boundaries contributes to lower the melting point of these boundaries. In this case Sr^{2+} ($r = 1.44$ Å) is replaced by Na^+ ($r > 1.44$ Å) and Bi^{3+} ($r < 1.44$ Å) [50], so the rate of diffusion to grain boundaries of Sr^{2+} is lower than that of Bi^{3+} and faster than that of Na^+. So, Bi^{3+} will diffuse better to grain boundaries than Sr^{2+}. As Bi^{3+} is a flux, it enhances grain growth.

Second, the grain size for all compositions increases when sintering temperature increases up to 800 ℃. Grain growth is a temperature dependent phenomenon. While the rate of the ion diffusion to the grain boundaries increases, the sintering temperature increases. The important driving forces for the mechanism in general are: excess free energy in a grain boundary which makes the grain to minimize its local surface area, and the volume free energy difference between the neighboring grains on either side of a grain boundary [51]. Shirsath *et al*. [52] correlated the increasing particle size with increasing sintering temperature to the coalescence that increases as sintering temperature increases. According to the phenomenological kinetic grain growth equation, the increase in sintering temperature increases the grain size [53]. This behavior of grain growth is in accord with the shrinkage increase, to explain that, shrinkage necessarily involves movement of the grain boundaries, and this movement must be in such a direction that the total area of boundaries decreases, so the shrinkage must thus be accompanied by grain growth [54]. In addition, the growth grain obeys the Arrhenius law [55]:

$$G_s = G_0 \exp[-A/(R \times T)] \quad (9)$$

where G_0 is the grain size before sintering; G_s is the grain size after sintering; A is the activation energy of grain growth; R denotes the ideal gas constant; and T is the sintering temperature.

This Arrhenius model describes the interplay between densification and grain size; accordingly, with increasing sintering temperature at the same holding time, crystal boundaries migrate more quickly. Thus, the microstructure is denser and the average grain size increases with the increase of sintering temperature. The logarithms of average grain versus reciprocal of sintering temperature are plotted in Fig. 7 by linear fitting for all solid solutions. Therefore, the effective activation energies of grain growth can be obtained by calculating the slope of $\ln(G_s/G_0)$ versus $1000/T$ and the results are 135.64 kJ/mol, 122.46 kJ/mol, 99.78 kJ/mol, 93.25 kJ/mol and 63.21 kJ/mol for $x =$ 0.0, 0.2, 0.5, 0.8 and 1.0, respectively. Compared to SBN, $Na_{0.5}Bi_{0.5}$ doping indeed reduces the activation energy as shown in Fig. 8. The more Sr is replaced by $Na_{0.5}Bi_{0.5}$, the lower the activation energy is and the easier the reaction of densification is. According to the sintering theory [56], the activation energy of sintering should be consistent with that of the diffusion of the rate-limiting species of sintering. In sintering polycrystalline ceramics, it is common that both grain boundary and lattice diffusion of the rate-limiting species can simultaneously contribute to densification [57]. In other words, generally the kinetics is limited either by the rate of chemical reaction or by the rate of diffusion phenomenon. In the former case, activation energy is very high. In our case, only the diffusion phenomenon is involved, which would explain why obtained activation energies for the grain growth of all solid solutions are relatively low (between 135 kJ/mol and 63 kJ/mol). The densification takes place through a faster diffusion process and results in an early lower

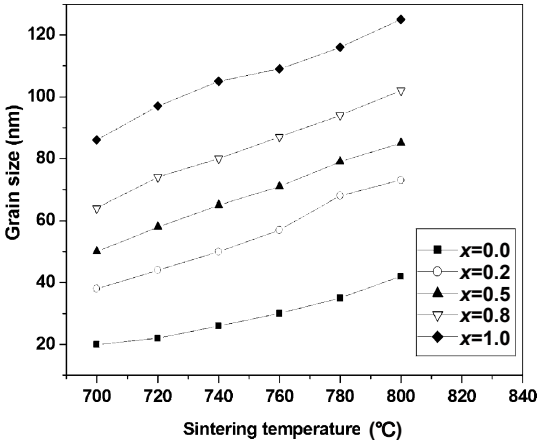

Fig. 6 Mean grain size as function of sintering temperature for $Sr_{1-x}(Na_{0.5}Bi_{0.5})_xBi_2Nb_2O_9$ solid solutions.

temperature sintering (800 ℃). This attitude is similar to that observed by Jardiel *et al*. [58], who indicated that activation energies of sintered $Bi_4Ti_3O_{12}$ prepared by coprecipitation method are lower than those energies calculated for compositions prepared by the solid state synthesis.

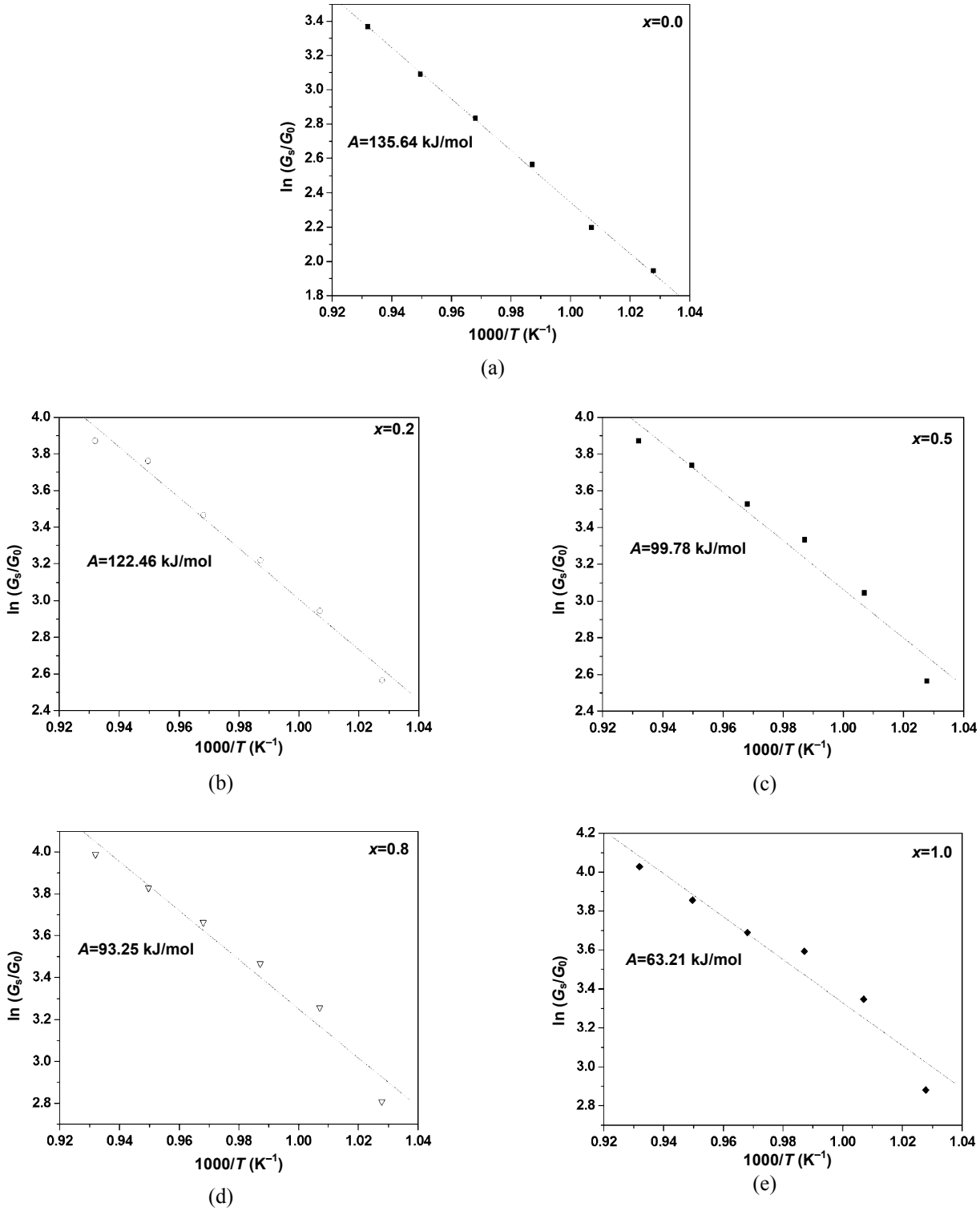

Fig. 7 Logarithm of average grain versus reciprocal of sintering temperature for $Sr_{1-x}(Na_{0.5}Bi_{0.5})_xBi_2Nb_2O_9$ solid solutions.

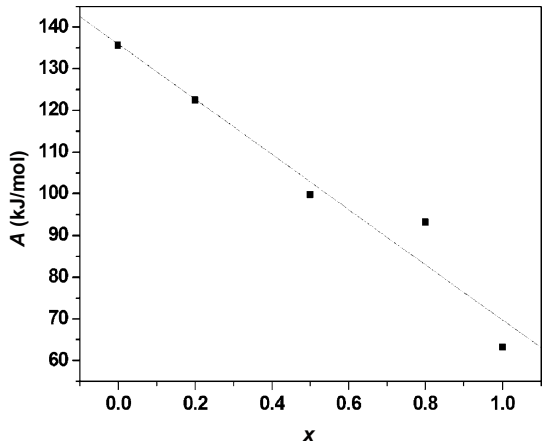

Fig. 8 Activation energy of grain growth as function of composition.

After 820 ℃, the sintering behavior begins to deteriorate due to exaggerated $Sr_{1-x}(Na_{0.5}Bi_{0.5})_xBi_2Nb_2O_9$ grain growth [59].

3.2 Impedance spectroscopy

Figure 9 shows the sintering temperature dependence on dielectric constant (ε_r) at 1 kHz frequency for $Sr_{1-x}(Na_{0.5}Bi_{0.5})_xBi_2Nb_2O_9$ ceramics. As can be seen, the permittivity is affected significantly by sintering temperature and compositions. For each value of x, ε_r increases up to 800 ℃.

On one hand, the relationships between ε_r values and sintering temperatures exhibit the similar trend as that between sintered densities and sintering temperatures. This attitude can be explained by the increase in density and in grain size as the sintering temperature is increased [60–62]. The raise in dielectric constant may be attributed to the mobile charge carriers related to oxygen vacancies [63]. In addition, agglomerations of powders become a resistant for ions to polarize between grains and grain boundaries [64]. According to our recent study, the dielectric constant of these compounds is only due to ionic polarization [37]. Theoretically, permittivity is related to ion polarizabilities by the Clausius–Mosotti equation [65]. It is believed that polarization of ions in grains may increase with grain necking growth.

On the other hand, the ε_r values increase with increasing the $Na_{0.5}Bi_{0.5}$ content. Maximum dielectric constant value of 384 is found for $Na_{0.5}Bi_{2.5}Nb_2O_9$ in ceramic sintered at 800 ℃. This behavior was explained in our recent work [37].

An increase in Curie temperature for $Sr_{1-x}(Na_{0.5}Bi_{0.5})_xBi_2Nb_2O_9$ ceramics with the increase of sintering temperature is observed (Fig. 10). Su *et al*. [66] determined that the behavior of Curie temperature can be related to microstructure, lattice defect, porosity, grain size, etc. Generally, the free energy of the ferroelectric phase increases and Curie temperature decreases with the increase of internal stress which can be relieved by pores [67]. Therefore, the ceramics with a lower density should have a higher T_C than the dense samples. In the dense ceramics with small amounts of pores, internal stress is mainly relieved by grain-boundary sliding [67]. In our case, the increase in Curie temperature with sintering suggests that the effect of internal stress relief by grain-boundary sliding

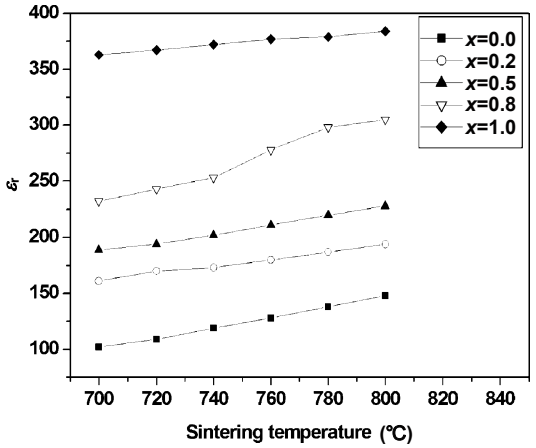

Fig. 9 Dielectric constant as function of sintering temperature for $Sr_{1-x}(Na_{0.5}Bi_{0.5})_xBi_2Nb_2O_9$ solid solutions.

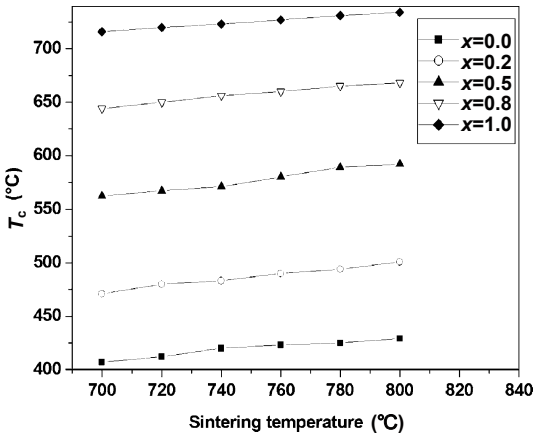

Fig. 10 Curie temperature as function of sintering temperature for $Sr_{1-x}(Na_{0.5}Bi_{0.5})_xBi_2Nb_2O_9$ solid solutions.

is more than the reduction of internal stress by pores. Mishra *et al*. [68] observed the similar behavior in BZT–BCT ceramics. The Curie temperature of the samples may be strongly affected by the grain size [69–71].

3. 3 Electrical studies

Firstly, it is worth knowing that a closer examination of the structure of SBN has revealed the existence of the vacancy; in order to compensate for the vacancy charge defects of opposite sign, oxygen vacancies are created to maintain the charge neutrality on the whole [72].

Electrical conductivities versus temperature at different sintering temperatures between 700 ℃ and 800 ℃, for $Sr_{1-x}(Na_{0.5}Bi_{0.5})_xBi_2Nb_2O_9$ are plotted in

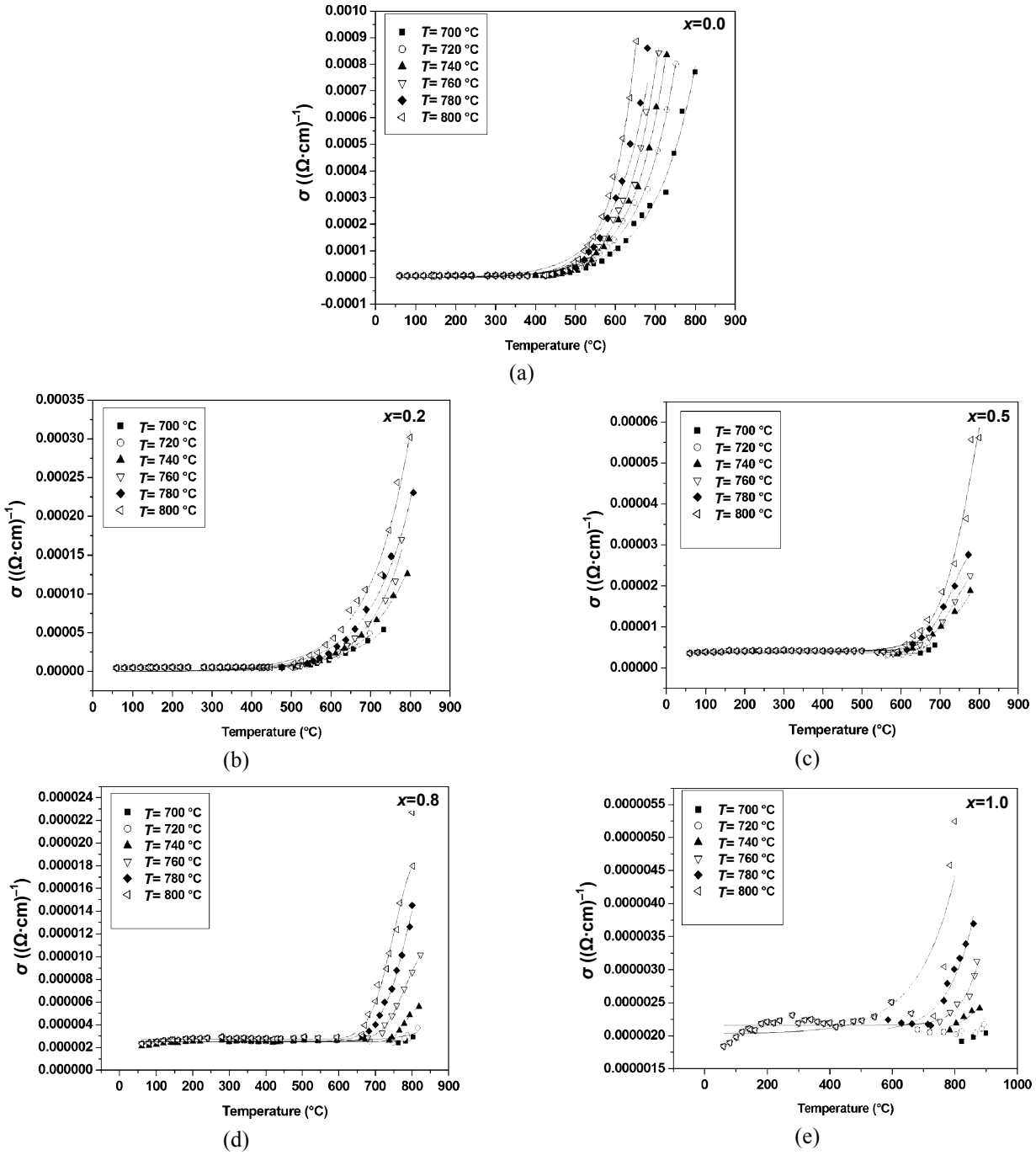

Fig. 11 Electrical conductivity as function of temperature at different sintering temperatures for $Sr_{1-x}(Na_{0.5}Bi_{0.5})_xBi_2Nb_2O_9$ solid solutions.

Fig. 11. The nature of curves shows that the conductivity increases with temperature. This suggests the presence of negative temperature coefficient of resistance (NTCR), a characteristic of dielectrics [73]. Activation energies (E_a) for conductivity are calculated from the Arrhenius relation for thermally activated conduction which is given as activated conduction (Eq. (8)). The linear fit is applied for the conductivity data using the least square fitting technique. It can be seen from Fig. 12 that for all

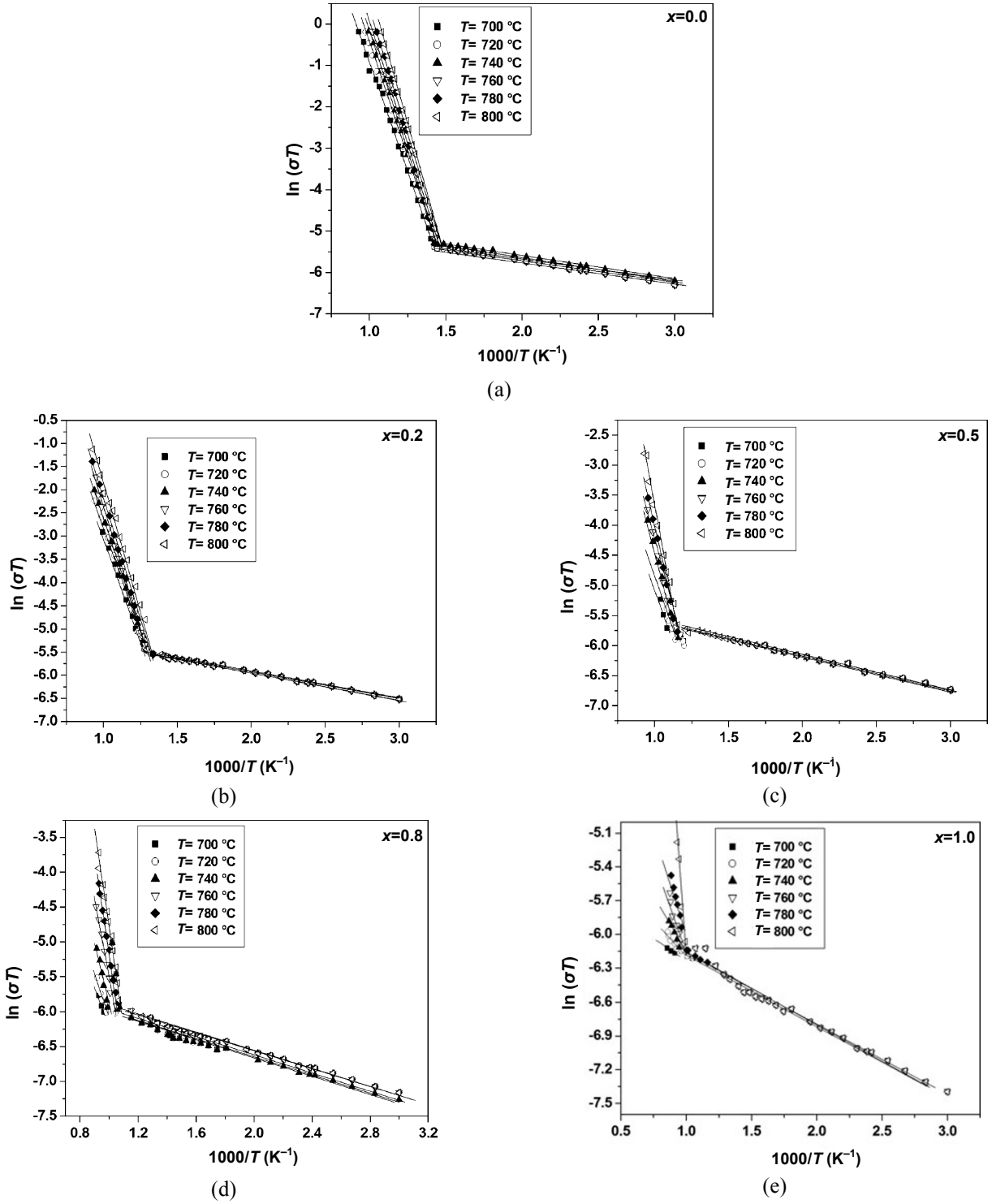

Fig. 12 Arrhenius plots of electrical conductivities as function of temperature for $Sr_{1-x}(Na_{0.5}Bi_{0.5})_xBi_2Nb_2O_9$ solid solutions.

samples the value of $\ln(\sigma T)$ increases almost linearly with increasing temperature up to a certain temperature at which a change of slope has occurred. This temperature corresponds to Curie point. It is observed that the transition temperatures are very close to those in impedance measurements. Such change in the slope is also due to the change of conduction mechanism from grain boundary to intragrain with the increase of temperature. There are two predominant conduction mechanisms. At low temperature region (ferroelectric phase), the conduction is dominant by extrinsic conduction, whereas the conduction at the high temperature (paraelectric phase) is dominated by the intrinsic conduction [74–76]. The activation energy is assumed to be the energy necessary to create and move vacancies [77,78]. At low temperatures, when the extrinsic conduction is predominant, the nominal activation energy equals diffusion activation energy (E_d). However, at high temperatures when intrinsic conduction predominates, the nominal activation is the sum of diffusion activation energy (E_d), and the formation energy of charge carrier (E_f) [10]:

$$E_a = E_d + E_f \quad (10)$$

The effect of sintering temperature in electrical conductivity can be also explained on the basis of microstructural changes, mainly coming from the enhancement of the densification [79].

It is also worth noting that, the activation energy of pure SBN of an earlier report by conventional sintered method [74,80] is higher than the current reported ceramic sintered at 800 ℃ after hydrothermal method.

4 Conclusions

The hydrothermal route has an interesting advantage for the synthesis of $Sr_{1-x}(Na_{0.5}Bi_{0.5})_xBi_2Nb_2O_9$ ($x = 0.0$, 0.2, 0.5, 0.8 and 1.0) powders consisting in low sintering temperature. An optimum lower sintering temperature equal to 800 ℃ is sufficient enough to give suitable properties. The effects of sintering at different temperatures on density, grain size and dielectric properties, for all solid solutions are studied. The results indicate that the values of sintered density, shrinkage and grain size are all in agreement. With the increase in sintering temperature, the density and the grain size increase. The activation energy for grain growth is determined. Values of ε_r increase with the increase of sintering temperature. The Curie temperature is progressively higher with increasing grain size. The electrical data indicate that the conductivity with different sintering is essentially due to the oxygen vacancies. The low sintering temperature of $Sr_{1-x}(Na_{0.5}Bi_{0.5})_xBi_2Nb_2O_9$ ceramics seems to be attractive for industrial purpose. It will allow their application to multilayer devices and will play an important role in the fabrication process to meet the requirement of miniaturization and integration.

References

[1] Wang PE, Chaki TK. Sintering behaviour and mechanical properties of hydroxyapatite and dicalcium phosphate. *J Mater Sci*: *Mater M* 1993, **4**: 150–158.

[2] Gökçe A, Findik F. Mechanical and physical properties of sintered aluminum powders. *Journal of Achievements in Materials and Manufacturing Engineering* 2008, **30**: 157–164.

[3] Mohan CRK, Bajpai PK. Effect of sintering optimization on the electrical properties of bulk $Ba_xSr_{1-x}TiO_3$ ceramics. *Physica B* 2008, **403**: 2173–2188.

[4] Hallmann L, Ulmer P, Reusser E, *et al*. Effect of dopants and sintering temperature on microstructure and low temperature degradation of dental Y-TZP-zirconia. *J Eur Ceram Soc* 2012, **32**: 4091–4104.

[5] Shaw NJ. Densification and coarsening during solid state sintering of ceramics: A review of the models III. Coarsening. *Int J Powder Metall* 1989, **21**: 25–29.

[6] Coondoo I, Jha AK, Agarwal SK. Enhancement of dielectric characteristics in donor doped Aurivillius $SrBi_2Ta_2O_9$ ferroelectric ceramics. *J Eur Ceram Soc* 2007, **27**: 253–260.

[7] Kajewski D, Ujma Z, Szot K, *et al*. Dielectric properties and phase transition in $SrBi_2Nb_2O_9$–$SrBi_2Ta_2O_9$ solid solution. *Ceram Int* 2009, **35**: 2351–2355.

[8] Wu W, Liang S, Wang X, *et al*. Synthesis, structures and photocatalytic activities of microcrystalline

ABi$_2$Nb$_2$O$_9$ (A = Sr, Ba) powders. *J Solid State Chem* 2011, **184**: 81–88.

[9] Panda AB, Tarafdar A, Pramanik P. Synthesis, characterization and properties of nano-sized $SrBi_2Ta_2O_9$ ceramics prepared by chemical routes. *J Eur Ceram Soc* 2004, **24**: 3043–3048.

[10] Dhak D, Dhak P, Pramanik P. Influence of substitution on dielectric and impedance spectroscopy of $Sr_{1-x}Bi_{2+y}Nb_2O_9$ ferroelectric ceramics synthesized by chemical route. *Appl Surf Sci* 2008, **254**: 3078–3092.

[11] Prasanta D, Debasis D, Kausikisankar P, *et al*. Studies of structural and electrical properties of $Ca_{1-x}Bi_{2+y}Nb_2O_9$ [$0.0 \leqslant x \leqslant 0.4$; $0.000 \leqslant y \leqslant 0.266$] ferroelectric ceramics prepared by organic precursor decomposition method. *Solid State Sci* 2008, **10**: 1936–1946.

[12] Júnior NLA, Simões AZ, Cavalheiro AA, *et al*. Structural and microstructural characterization of $SrBi_2(Ta_{0.5}Nb_{0.48}W_{0.02})_2O_9$ powders. *J Alloys Compd* 2008, **454**: 61–65.

[13] Gaikwad SP, Dhage SR, Potdar HS, *et al*. Co-precipitation method for the preparation of nanocrystalline ferroelectric $SrBi_2Nb_2O_9$ ceramics. *J Electroceram* 2005, **14**: 83–87.

[14] Gaikwad SP, Potdar HS, Samuel V, *et al*. Co-precipitation method for the preparation of fine ferroelectric $BaBi_2Nb_2O_9$. *Ceram Int* 2005, **31**: 379–381.

[15] Radha R, Gupta UN, Samuel V, *et al*. A co-precipitation technique to prepare $BiNbO_4$ powders. *Ceram Int* 2008, **34**: 1565–1567.

[16] Kato K, Zheng C, Finder JM, *et al*. Sol–gel route to ferroelectric layer-structured perovskite $SrBi_2Ta_2O_9$ and $SrBi_2Nb_2O_9$ thin films. *J Am Ceram Soc* 1998, **81**: 1869–1875.

[17] Nelis D, Van Werde K, Mondelaers D, *et al*. Aqueous solution–gel synthesis of strontium bismuth niobate ($SrBi_2Nb_2O_9$). *J Sol–Gel Sci Technol* 2003, **26**: 1125–1129.

[18] Zanetti SM, Santiago EI, Bulhões LOS, *et al*. Preparation of characterization of nanosized $SrBi_2Nb_2O_9$ powder by the combustion synthesis. *Mater Lett* 2003, **57**: 2812–2816.

[19] Lu C-H, Chen Y-C. Sintering and decomposition of ferroelectric layered perovskites: Strontium bismuth tantalate ceramics. *J Eur Ceram Soc* 1999, **19**: 2909–2915.

[20] Chen D, Liu Y, Li Y, *et al*. Low-temperature sintering of M-type barium ferrite with $BaCu(B_2O_5)$ additive. *J Magn Magn Mater* 2012, **324**: 449–452.

[21] Liu H, Li Q, Ma J, *et al*. Effects of Bi^{3+} content and grain size on electrical properties of $SrBi_2Ta_2O_9$ ceramic. *Mater Lett* 2012, **76**: 21–24.

[22] Iqbal Y, Jamal A, Ullah R, *et al*. Effect of fluxing additive on sintering temperature, microstructure and properties of $BaTiO_3$. *Bull Mater Sci* 2012, **35**: 387–394.

[23] Zhang P, Hua Y, Xia W, *et al*. Effect of H_3BO_3 on the low temperature sintering and microwave dielectric properties of $Li_2ZnTi_3O_8$ ceramics. *J Alloys Compd* 2012, **534**: 9–12.

[24] Zhang G, Liu S, Yu Y, *et al*. Microstructure and electrical properties of $(Pb_{0.87}Ba_{0.1}La_{0.02})(Zr_{0.68}Sn_{0.24}Ti_{0.08})O_3$ anti-ferroelectric ceramics fabricated by the hot-press sintering method. *J Eur Ceram Soc* 2013, **33**: 113–121.

[25] Nygren M, Shen Z. On the preparation of bio-, nano- and structural ceramics and composites by spark plasma sintering. *Solid State Sci* 2003, **5**: 125–131.

[26] Li J-F, Wang K, Zhang B-P, *et al*. Ferroelectric and piezoelectric properties of fine-grained $Na_{0.5}K_{0.5}NbO_3$ lead-free piezoelectric ceramics prepared by spark plasma sintering. *J Am Ceram Soc* 2006, **89**: 706–709.

[27] Polotai A, Breece K, Dickey E, *et al*. A novel approach to sintering nanocrystalline barium titanate ceramics. *J Am Ceram Soc* 2005, **88**: 3008–3012.

[28] Wang X-H, Deng X-Y, Bai H-L, *et al*. Two-step sintering of ceramics with constant grain-size, II: $BaTiO_3$ and Ni–Cu–Zn ferrite. *J Am Ceram Soc* 2006, **89**: 438–443.

[29] Fang J, Wang X, Tian Z, *et al*. Two-step sintering: An approach to broaden the sintering temperature range of alkaline niobate-based lead-free piezoceramics. *J Am Ceram Soc* 2010, **93**: 3552–3555.

[30] Senthil V, Badapanda T, Bose AC, *et al*. Impedance and electrical modulus study of microwave-sintered $SrBi_2Ta_2O_9$ ceramic. *ISRN Ceramics* 2012, **2012**: 943734.

[31] Lu SW, Lee BI, Wang ZL, *et al*. Hydrothermal synthesis and structural characterization of $BaTiO_3$ nanocrystals. *J Cryst Growth* 2000, **219**: 269–276.

[32] Dias A, Buono VTL, Ciminelli VST, *et al*. Hydrothermal synthesis and sintering of electroceramics. *J Eur Ceram Soc* 1999, **19**: 1027–1030.

[33] Li L, Gong Y-Q, Gong L-J, *et al*. Low-temperature hydro/solvothermal synthesis of Ta-modified $K_{0.5}Na_{0.5}NbO_3$ powders and piezoelectric properties of corresponding ceramics. *Mater Design* 2012, **33**: 362–366.

[34] Hotta Y, Duran C, Sato K, *et al*. Densification and grain growth in $BaTiO_3$ ceramics fabricated from

nanopowders synthesized by ball-milling assisted hydrothermal reaction. *J Eur Ceram Soc* 2008, **28**: 599–604.

[35] Venkataraman BH, Varma KBR. Impedance and dielectric studies of ferroelectric $SrBi_2Nb_2O_9$ ceramics. *J Phys Chem Solids* 2003, **64**: 2105–2112.

[36] Pookmanee P, Rujijanagul G, Ananta S, *et al*. Effect of sintering temperature on microstructure of hydrothermally prepared bismuth sodium titanate ceramics. *J Eur Ceram Soc* 2004, **24**: 517–520.

[37] Naceur H, Megriche A, Maaoui ME. Structural distortion and dielectric properties of $Sr_{1-x}(Na_{0.5}Bi_{0.5})_xBi_2Nb_2O_9$ ($x = 0.0$, 0.2, 0.5, 0.8 and 1.0). *J Alloys Compd* 2013, **46**: 145–150.

[38] Aoyagi R, Takeda H, Okamura S, *et al*. Synthesis and electrical properties of sodium bismuth niobate $Na_{0.5}Bi_{2.5}Nb_2O_9$. *Mater Res Bull* 2003, **38**: 25–32.

[39] Einstein A. Eine neue Bestimmung der Moleküldimensionen. *Annalen der Physik* 1906, **324**: 289–306.

[40] Garcia DE, Klein AN, Hotza D. Advanced ceramics with dense and fine-grained microstructures through fast firing. *Rev Adv Mater Sci* 2012, **30**: 273–281.

[41] Wang Q, Wang Q, Zhang X, *et al*. The effect of sintering temperature on the structure and degradability of strontium-doped calcium polyphosphate bioceramic. *Ceram-Silikaty* 2010, **54**: 97–102.

[42] Krishnan K, Sahay SS, Singh S, *et al*. Modeling the accelerated cyclic annealing kinetics. *J Appl Phys* 2006, **100**: 093505.

[43] Hungría T, Galy J, Castro A. Spark plasma sintering as a useful technique to the nanostructuration of piezo-ferroelectric materials. *Adv Eng Mater* 2009, **11**: 615–631.

[44] Hu M, Luo C, Tian H, *et al*. Phase evolution, crystal structure and dielectric behavior of $(1-x)Nd(Zn_{0.5}Ti_{0.5})O_3+xBi(Zn_{0.5}Ti_{0.5})O_3$ compound ceramics. *J Alloys Compd* 2011, **509**: 2993–2999.

[45] Skidmore TA, Milne SJ. Phase development during mixed-oxide processing of a $[Na_{0.5}K_{0.5}NbO_3]_{1-x}$–$[LiTaO_3]_x$ powder. *J Mater Res* 2007, **22**: 2265–2272.

[46] Rivas-Vázquez LP, Rendón-Angeles JC, Rodríguez-Galicia JL, *et al*. Preparation of calcium doped $LaCrO_3$ fine powders by hydrothermal method and its sintering. *J Eur Ceram Soc* 2006, **26**: 81–88.

[47] Mandoki NT, Courtois C, Champagne P, *et al*. Hydrothermal synthesis of doped PZT powders: Sintering and ceramic properties. *Mater Lett* 2004, **58**: 2489–2493.

[48] Yahya N, Masoud RAH, Daud H, *et al*. Synthesis of $Al_3Fe_5O_{12}$ cubic structure by extremely low sintering temperature of sol gel technique. *Am J Engg & Applied Sci* 2009, **2**: 76–79.

[49] Cahn JW. The impurity-drag effect in grain boundary motion. *Acta Metall* 1962, **10**: 789–798.

[50] Shannon RD. Revised effective ionic radii and systematic studies of interatomic distances in halides and chalcogenides. *Acta Cryst* 1976, **A32**: 751–767.

[51] Floro JA, Thompson CV, Carel R, *et al*. Competition between strain and interface energy during epitaxial grain growth in Ag films on Ni(001). *J Mater Res* 1994, **9**: 2411–2424.

[52] Shirsath SE, Kadam RH, Gaikwad AS, *et al*. Effect of sintering temperature and the particle size on the structural and magnetic properties of nanocrystalline $Li_{0.5}Fe_{2.5}O_4$. *J Magn Magn Mater* 2011, **323**: 3104–3108.

[53] Cortés J, Valencia E. Phenomenological equations of the kinetics of heterogeneous adsorption with interaction between adsorbed molecules. *Phys Rev B* 1995, **51**: 2621–2623.

[54] Budworth DW. The selection of grain-growth control additives for the sintering of ceramic. *Mineral Mag* 1970, **37**: 833–838.

[55] Coble RL. Sintering crystalline solids. I. Intermediate and final state diffusion models. *J Appl Phys* 1961, **32**: 787–792.

[56] Dosdale T, Brook RJ. Comparison of diffusion data and of activation energies. *J Am Ceram Soc* 1983, **66**: 392–395.

[57] Fang T-T, Shiue J-T, Shiau F-S. On the evaluation of the activation energy of sintering. *Mater Chem Phys* 2003, **80**: 108–113.

[58] Jardiel T, Caballero AC, Villegas M. Sintering kinetic of $Bi_4Ti_3O_{12}$ based ceramics. *Bol Soc Esp Ceram* 2006, **45**: 202–206.

[59] Kan Y, Wang P, Li Y, *et al*. Low-temperature sintering of $Bi_4Ti_3O_{12}$ derived from co-precipitation method. *Mater Lett* 2002, **56**: 910–914.

[60] Wu A, Vilarinho PM, Salvado IMM, *et al*. Sol–gel preparation of lead zirconate titanate powders and ceramics: Effect of alkoxide stabilizers and lead precursors. *J Am Ceram Soc* 2000, **83**: 1379–1385.

[61] Shaikh PA, Kolekar YD. Study of microstructural, electrical and dielectric properties of perovskite (0.7) PMN–(0.3) PT ferroelectric at different sintering temperatures. *J Anal Appl Pyrol* 2012, **93**: 41–46.

[62] Prasad KVR, Raju AR, Varma KBR. Grain size effects on the dielectric properties of ferroelectric $Bi_2VO_{5.5}$ ceramics. *J Mater Sci* 1994, **29**: 2691–2696.

[63] Cheng ZX, Wang XL, Dou SX, *et al*. Ferroelectric properties of $Bi_{3.25}Sm_{0.75}V_{0.02}T_{2.98}O_{12}$ thin film at

elevated temperature. *Appl Phys Lett* 2007, **90**: 222902.

[64] Yan LC, Hassan J, Hashim M, *et al*. Effect of sintering temperatures on the microstructure and dielectric properties of $SrTiO_3$. *World Appl Sci J* 2011, **15**: 1614–1618.

[65] Shannon RD. Dielectric polarizabilities of ions in oxides and fluorides. *J Appl Phys* 1993, **73**: 348–366.

[66] Su H, Zhang H, Tang X, *et al*. High-permeability and high-Curie temperature NiCuZn ferrite. *J Magn Magn Mater* 2004, **283**: 157–163.

[67] Chen XM, Ma HY, Ding W, *et al*. Microstructure, dielectric, and piezoelectric properties of $Pb_{0.92}Ba_{0.08}Nb_2O_6$–0.25 wt% TiO_2 ceramics: Effect of sintering temperature. *J Am Ceram Soc* 2011, **94**: 3364–3372.

[68] Mishra P, Sonia, Kumar P. Effect of sintering temperature on dielectric, piezoelectric and ferroelectric properties of BZT–BCT 50/50 ceramics. *J Alloys Compd* 2012, **545**: 210–215.

[69] Bhuiyan MA, Hoque SM, Choudhury S. Effect of sintering temperature on microstructure and magnetic properties of $NiFe_2O_4$ prepared from nano size powder of NiO and Fe_2O_3. *Journal of Bangladesh Academy of Sciences* 2010, **34**: 189–195.

[70] Zhang Q, Zhang Y, Wang X, *et al*. Influence of sintering temperature on energy storage properties of $BaTiO_3$–$(Sr_{1-1.5x}Bi_x)TiO_3$ ceramics. *Ceram Int* 2012, **38**: 4765–4770.

[71] Wada N, Tanaka H, Hamaji Y, *et al*. Microstructures and dielectric properties of fine-grained $BaTiO_3$ ceramics. *Jpn J Appl Phys* 1996, **35**: 5141–5144.

[72] Chen T-C, Thio C-L, Desu SB. Impedance spectroscopy of $SrBi_2Ta_2O_9$ and $SrBi_2Nb_2O_9$ ceramics correlation with fatigue behavior. *J Mater Res* 1997, **12**: 2628–2637.

[73] Shrivastava V, Jha AK, Mendiratta RG. Structural and electrical studies in La-substituted $SrBi_2Nb_2O_9$ ferroelectric ceramics. *Physica B* 2006, **371**: 337–342.

[74] Forbess MJ, Seraji S, Wu Y, *et al*. Dielectric properties of layered perovskite $Sr_xA_{1-x}Bi_2Nb_2O_9$ ferroelectrics (with A = La, Ca and $x = 0$, 0.1). *Appl Phys Lett* 2000, **76**: 2934–2936.

[75] He LX, Yoo HI. Effects of B-site ion (M) substitution on the ionic conductivity of $(Li_{3x}La_{2/3-x})_{1+y/2}(M_yTi_{1-y})O_3$ (M = Al, Cr). *Electrochim Acta* 2003, **48**: 1357–1366.

[76] Kuang X, Allix MMB, Claridge JB, *et al*. Crystal structure, microwave dielectric properties and AC conductivity of B-cation deficient hexagonal perovskites $La_5M_xTi_{4-x}O_{15}$ ($x = 0.5$, 1; M = Zn, Mg, Ga, Al). *J Mater Chem* 2006, **16**: 1038–1045.

[77] Kröger FA. The chemistry of imperfect crystals. *J Appl Cryst* 1975, **8**: 497–498.

[78] Parkash OM, Mandal KD, Christopher CC, *et al*. Electrical behaviour of lanthanum- and cobalt-doped strontium stannate. *Bull Mater Sci* 1994, **17**: 253–257.

[79] Kant R, Singh K, Pandey OP. Microstructural and electrical behavior of $Bi_4V_{2-x}Cu_xO_{11-\delta}$ ($0 \leqslant x \leqslant 0.4$). *Ceram Int* 2009, **35**: 221–227.

[80] Wang XP, Fang QF. Mechanical and dielectric relaxation studies on the mechanism of oxygen ion diffusion in $La_2Mo_2O_9$. *Phys Rev B* 2002, **65**: 064304.